ω Meson from lattice QCD

Haobo Yan (燕浩波),[1, 2, *] Maxim Mai,[2, 3, 4, †] Marco Garofalo,[2, ‡]
Ulf-G. Meißner,[2, 5, 6, §] Chuan Liu,[1, 7, 8, ¶] Liuming Liu,[9, 10, **] and Carsten Urbach[2, ††]

[1] *School of Physics, Peking University, Beijing 100871, China*
[2] *Helmholtz-Institut für Strahlen- und Kernphysik (Theorie) and Bethe*
Center for Theoretical Physics, Universität Bonn, 53115 Bonn, Germany
[3] *Albert Einstein Center for Fundamental Physics, Institute for Theoretical Physics,*
University of Bern, Sidlerstrasse 5, 3012 Bern, Switzerland
[4] *Institute for Nuclear Studies and Department of Physics,*
The George Washington University, Washington, DC 20052, USA
[5] *Institute for Advanced Simulation (IAS-4), Forschungszentrum Jülich, 52425 Jülich, Germany*
[6] *Peng Huanwu Collaborative Center for Research and Education, Beihang University, Beijing 100191, China*
[7] *Center for High Energy Physics, Peking University, Beijing 100871, China*
[8] *Collaborative Innovation Center of Quantum Matter, Beijing 100871, China*
[9] *Institute of Modern Physics, Chinese Academy of Sciences, Lanzhou 730000, China*
[10] *University of Chinese Academy of Sciences, Beijing 100049, China*

Many excited states in the hadron spectrum have large branching ratios to three-hadron final states. Understanding such particles from first principles QCD requires input from lattice QCD with one-, two-, and three-meson interpolators as well as a reliable three-body formalism relating finite-volume spectra at unphysical pion mass values to the scattering amplitudes at the physical point. In this work, we provide the first-ever calculation of the resonance parameters of the ω meson from lattice QCD, including an update of the formalism through matching to effective field theories. The main result of this pioneering study, the pole position of the ω meson at $\sqrt{s_\omega} = (778.0(11.2) - i\,3.0(5))\,\mathrm{MeV}$, agrees reasonably well with experiment. In addition we provide an estimate of the $\omega - \rho$ mass difference as $29(15)\,\mathrm{MeV}$.

Introduction–Quantum Chromodynamics (QCD), the theory of the strong interactions, not only explains the binding of quarks and gluons to protons and neutrons, which represent most of the visible matter around us, but also the full spectrum of the so-called hadrons. It consists in general of baryon and meson states, most of which are actually resonances. The $\omega(782)$ meson plays a special role in this hadron spectrum. First, it is the lightest hadron that features a strong, isospin conserving decay into three particles in the final state, $\omega \to 3\pi$. Second, within the vector dominance picture of the photon-nucleon interactions, it dominates the isoscalar response [1, 2] and combined with the topological soliton picture of the nucleon, it allows one to explain the difference in the baryonic charge and the isoscalar electric radius [3, 4]. Third, in the one-boson-exchange picture of the nucleon-nucleon interaction, it generates the observed repulsion at distances below 1 fm; see, e.g., [5, 6]. Fourth, due to strong isospin violation, it mixes with the $\rho(770)$ meson leading to marked effects in the pion vector form factor, see, e.g., [7, 8]. Finally, the $\omega - \rho$ mass splitting is phenomenologically interesting, for instance for the anomalous magnetic moment of the muon [9–11], or recently also in the context of dark matter and so-called mirror matter [12, 13]. For all these reasons, a first-principles calculation of this intriguing state based on QCD is called for.

The by now standard approach for such a nonperturbative calculation is represented by lattice QCD, where space-time is discretized, and the Euclidean path integral is estimated using Markov Chain Monte Carlo methods. While lattice QCD has already addressed systematically the lowest resonances, the $f_0(500)$ [14–23] and the $\rho(770)$ [24–42], which decay into two pions in the final state (for a review see [43]), there are only investigations of repulsive three-body systems [44–50], and only one exploratory lattice investigation of the $a_1(1260)$ axial meson decaying into three pions available so far [51]. In particular, there is no calculation of the complex pole position of the ω meson available, because it decays predominantly to three pions in the final state. The reason is that only in the last decade the required formalism for such types of lattice computations has become available, see recent reviews [52, 53]. Using one of the three state-of-the-art formalisms [54], we report here on the first lattice calculation of the $\omega(782)$ meson, thus filling in the gap mentioned before by providing the complex energy, namely the mass and the width of the ω. Owing to its three-pion decay, where two pions can form a ρ [55], the ω cannot be considered in isolation, and we thus rely on chiral Lagrangians with vector mesons (for a review, see [56]) in the analysis of the ω self-energy. In particular, we use effective field theory for the extrapolation to the physical pion mass value.

Lattice computation—The gauge configurations used in this work were generated by the CLQCD Collaboration with $N_\mathrm{f} = 2 + 1$ flavors of dynamical quarks using the tadpole-improved tree-level Symanzik gauge action and tadpole-improved tree-level Wilson clover fermions [57].

The results presented here are based on four ensembles at the same lattice spacing 0.07746(18) fm, with two pion masses $M_\pi \approx 208$ and 305 MeV, and two volumes each. The details of the ensembles are listed in Table I. Specifically, the two ensembles, F32P21/F48P21 (F32P30/F48P30), share the same pion mass and lattice spacing but differ in volume.

The lattice discretization reduces the continuum rotational symmetry to the cubic symmetry group O_h in the rest frame. Therefore, operators satisfying specific transformation laws of the cubic group are constructed to interpolate the ρ and the ω mesons. This study focuses on the irreducible representation (irrep) T_1^- for both isovector $\pi\pi$ and isoscalar $\pi\pi\pi$ in the rest frame, where the $\pi\pi$ system predominantly involves the ρ in the P wave and $\pi\pi\pi$ houses the ω. The constructed operators include types with a single meson, two mesons, and three mesons, projected to the proper isospin and the T_1^- irrep. For an efficient tool for operator construction, see `OpTion` [58]. We emphasize that it is necessary to have all three types of operators to overlap with the dynamical channels and the ω, and obtain reliable and precise energy spectra with minimal pollution from the higher energy region. The detailed form of the operators we used can be found in the Supplemental Material [59]. In order to extract the finite-volume spectra, the correlation matrices of a wide range of operators O_i, $C_{ij}(t) = \langle O_i t) O_j^\dagger(0)\rangle_T$ are diagonalized by solving a generalized eigenvalue problem [63–66]; see details in [59]. Lattice energy levels aE are extracted from the exponential decay of the principal correlators in Euclidean time. We note in passing that due to exact isospin symmetry in our lattice calculation the channel $\omega \to \pi^+\pi^-$ is forbidden, but accounts only for about 2% of the ω decays in total. We also note that there is mixing with the φ meson, which is, however, too high in energy to play a role in our analysis.

The number of quark contraction diagrams emerging in the construction of the relevant correlators grows factorially with the number of scattered particles. For instance, there are nine diagrams for $\pi\pi \to \pi\pi$ ($I = 0$) when both sink and source are two-body operators, but 202 in $\pi\pi\pi \to \pi\pi\pi$ ($I = 0$), with the topologies depicted in Fig. 1 and the Supplemental Material [59]. Besides the large number of diagrams, most of the diagrams include disconnected quark annihilation subdiagrams, which are difficult to calculate and induce a poor signal. Therefore, we employ the distillation method [67] to compute all-to-all quark perambulators, and construct C_{ij} from these.

The resulting $\pi\pi$ and $\pi\pi\pi$ finite-volume spectra are shown in Fig. 2. The ground levels appear in both $\pi\pi$ and $\pi\pi\pi$ channels below the first non interacting levels indicating strong attraction in both the ρ and ω channel. In the $\pi\pi\pi$ channel, at $M_\pi \approx 208$ MeV, the ground states are higher than threshold, indicating a resonance with nonzero phase space to decay; at $M_\pi \approx 305$ MeV, the

Ensemble	Volume	M_π/MeV	N_{confs}
F32P21	$32^3 \times 64$	206.8(2.1)	459
F48P21	$48^3 \times 96$	207.58(76)	221
F32P30	$32^3 \times 96$	303.61(71)	777
F48P30	$48^3 \times 96$	304.95(49)	201

TABLE I. CLQCD gauge configurations [57] used in this work with a lattice spacing of $a = 0.07746(18)$ fm. The quoted errors are purely statistical.
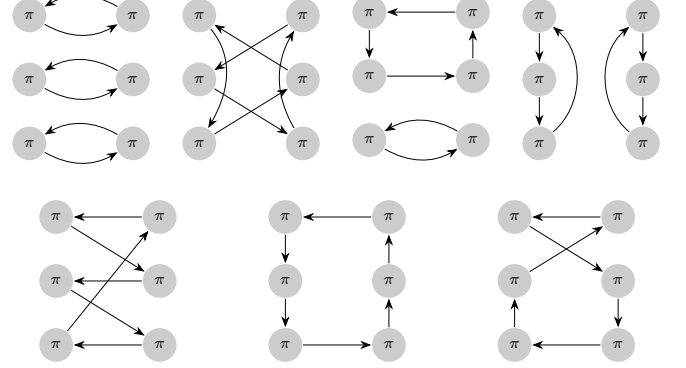

FIG. 1. A selection of diagram topologies for $I = 0$ for $\pi\pi\pi \to \pi\pi\pi$. All diagrams with the same source and sink are permutations and recombination of these topologies. The other topologies can be found in the Supplemental Material [59].

ground levels are consistent between the two volumes and lower than the $\pi\pi\pi$ threshold, indicating a bound state.

Quantization conditions and resonance parameter—The finite-volume spectra discussed above contain two- and three-particle dynamics to be decoded through appropriate quantization conditions. In this work, we utilize the finite-volume unitarity (FVU) approach [54] already applied to a variety of three-body systems [44, 49, 51, 68–71]. It was shown to be equivalent to the other two known three-body formalisms in theory in Ref. [72] and numerically in Ref. [70].

The dominant interaction channel of the ω system is formalized through the $\pi\rho$ channel in the relative P wave [55]. Thus, in the FVU formalism, the three-body finite-volume spectrum is predicted in the center-of-mass frame as a set of three-body energies $E_3 = \sqrt{s}$ for which

$$\det\{[\tilde{K}^{-1}(s) - \Sigma^{FV}(s)]E_L - [\tilde{B}(s) + \tilde{C}(s)]\}_{p'\lambda',p\lambda}^\Gamma = 0\,, \tag{1}$$

in the plane-wave adn helicity basis (PWH) $\{\pi(\boldsymbol{p})\rho_\lambda(-\boldsymbol{p})|\boldsymbol{p}L/(2\pi) \in \mathbb{Z}^3, \lambda \in \{-1, 0, +1\}\}$ while projecting each element of this equation to the T_1^- irrep of the O_h group; see [51, 73]. The matrices $\tilde{B}$ (one-pion exchange) and Σ^{FV} (self-energy of the ρ system in finite-volume) collect all on shell configurations of the three pions and, therefore, single out all power-law
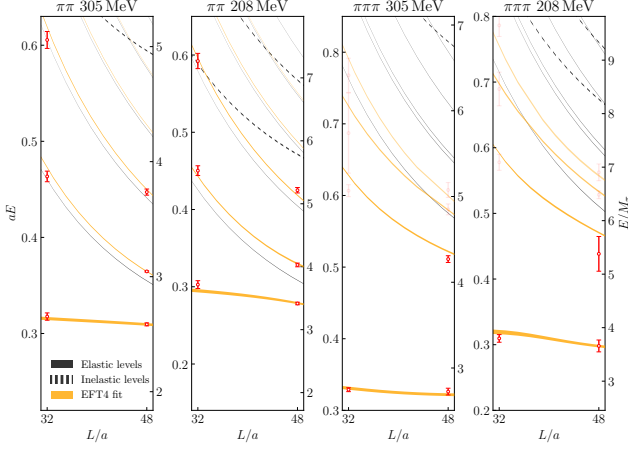
FIG. 2. Finite-volume spectra for $\pi\pi(I=1)$ and $\pi\pi\pi(I=0)$ for heavy and light pion mass. Red points represent the interacting lattice energy levels aE in units of the pion mass, the faded of which are not included in the analysis. Dashed and dot-dashed lines depict the non interacting elastic and inelastic levels. The orange bands are the solutions from the main fit.

volume dependence of this system. Together with the kinematical factor E_L these matrices are entirely fixed. Contrary to this, the matrices $\tilde{K}^{-1}$ and $\tilde{C}$ are volume-independent quantities (up to the neglected $e^{-M_\pi L}$ terms) containing information on the two- and three-body dynamics, respectively. The exponential effects from the small volume were examined by repeating the EFT4 fit excluding the levels from F32P21. We found that the difference from the original fit is of the order of the statistical error, and it is quoted as a systematic error in the Supplemental Material [59]. The two-body force provides access to the two-body energy eigenvalues through $\{E_2 \in \mathbb{R} | \tilde{K}^{-1} = \Sigma^{FV}, \boldsymbol{p}^{(\prime)} = \boldsymbol{0}\}$ which is equivalent to the usual Lüscher method [74] up to exponentially suppressed terms. While, in general, $\tilde{K}^{-1}$ and $\tilde{C}$ are not known, various choices relevant for the ρ and ω systems, relying on a generic parametrization and effective field theory are discussed below.

Generic method (GEN): the two-body force is parametrized as $[\tilde{K}^{-1}]_{\boldsymbol{p}'\lambda',\boldsymbol{p}\lambda} = \delta_{\lambda'\lambda}\delta_{\boldsymbol{p}'\boldsymbol{p}}\sum_{i=0}^{N}a_i\sigma_p^i$ for the two-body invariant mass $\sigma_p := s + M_\pi^2 - 2\sqrt{s}\sqrt{\boldsymbol{p}^2 + M_\pi^2}$ ($E_2 = \sqrt{\sigma_0}$) and a spectator momentum $\boldsymbol{p}$. We found that $N=1$ is entirely sufficient to describe the available lattice input, and this is also mathematically equivalent to the usual Breit-Wigner form. Similarly, the three-body force $\tilde{C}$ is parametrized through a general expansion in the orbital angular momentum (JLS) basis ($\pi\rho$ in relative P wave) $\tilde{c}_{11} = \frac{c_0}{s-M_\omega^2} + c_1 + ...$ and then mapped to the PWH [71, 75, 76]. Here again, the order of the expansion depends on the availability and precision of the input. In the current case a two-parameter fit (c_0, M_ω) turned out as sufficiently flexible.

Effective field theory (EFT): The GEN methodology does not allow for chiral extrapolation to the physical point which can be circumvented through EFTs as widely used in the two-body sector [53, 77] but not yet in studies of three-hadron resonances from the lattice. Still, continuum results on $\omega \to \pi\pi\pi$ and $\rho \to \pi\pi$ have existed for several decades, see the review [56]. Using the results quoted in that review we perform a matching on the level of $2 \to 2$ and $3 \to 3$ scattering amplitudes. A somewhat lengthy but straightforward calculation at the tree-level yields

$$\left[\tilde{K}^{-1}\right]_{\boldsymbol{p}'\lambda',\boldsymbol{p}\lambda} = \delta_{\lambda'\lambda}\delta_{\boldsymbol{p}'\boldsymbol{p}}\frac{\sigma_p - M_\rho^2}{2g^2},$$
$$\tilde{c}_{11} = \frac{6s(M_\rho^2 - \sigma_q + 6g^2f_\pi^2)(M_\rho^2 - \sigma_p + 6g^2f_\pi^2)}{64g^2\pi^3 f_\pi^6(s - M_\omega^2)}, \quad (2)$$

where the latter is expressed in the JLS basis, projected to the PWH basis [71, 75, 76]. Throughout this derivation, we have assumed that two- and three-pion interactions are saturated by the s-channel resonance exchange (justified by the narrow width of the ρ and ω mesons) and set $g_{\rho\pi\pi} = g_{\omega\rho\pi} = g$ following [56]. Thus far, the matching relations of Eq. (2) provide access to the two- and three-body force for given (g, M_ρ, M_ω). The Kawarabayashi-Suzuki-Fayyazuddin-Riazzudin (KSFR) relation [78, 79] allows one to reduce this set further through $M_\rho = \sqrt{2}gf_\pi$. Indeed, this specifies already a chiral (M_π) extrapolation through the $f_\pi(M_\pi)$ from chiral perturbation theory [80]. Using the generalized KSFR relation but allowing for a pion-mass independent shift $M_\omega := M_\rho + \delta = \sqrt{2}gf_\pi + \delta$ defines the EFT2 method referring to free parameters (g, δ). Abandoning the KSFR relation entirely we define the EFT4 method by $M_\rho = M_V + a M_\pi^2$, $M_\omega = M_V + a M_\pi^2 + \delta$ [81, 82], leaving us with four free parameters (g, M_V, a, δ). Clearly, the proposed EFT methods only represent a larger class of EFTs with heavy degrees of freedom [3]. Ultimately, the defined method will be tested against lattice QCD results.

The three-body parameters obtained through a fit to the lattice spectra will be used to obtain the universal parameters of the ρ and ω mesons through their pole positions on the second Riemann sheet. The necessary framework is provided through the infinite-volume unitarity (IVU) approach [54, 83] corresponding to the above quantization conditions. The part of the scattering amplitude relevant to the emergence of resonance poles is obtained through an integral equation,

$$T = \tilde{B} + \tilde{C} + \int \frac{d^3l}{(2\pi)^3} \frac{\tilde{B} + \tilde{C}}{2E_l(\tilde{K}^{-1} - \Sigma^{IV})}T, \quad (3)$$

where we have suppressed kinematic arguments for brevity; see Eq. (1) and [51, 71, 84]. Here, Σ^{IV} denotes the usual ρ self-energy integral. The corresponding integral equation can be solved through a complex contour

deformation in the JLS basis [71, 76, 85], and pole positions extracted as shown in [51, 70, 84]. The corresponding procedure for finding two-body resonance poles boils down to finding solutions $\{E_2 \in \mathbb{C} | \tilde{K}^{-1} = \Sigma^{IV}\}$ on the second Riemann sheet.

The three-body quantization condition is necessarily formulated [53] as an infinitely dimensional determinant equation (PWH). Throughout, this work we assume all momenta up to $\boldsymbol{p}_{\max} = (2\pi)/L(0,1,1)$ for computational reasons. Related to this is also the fact that for smaller volumes the spectator momentum cutoff leads to negative values of the two-body invariant mass. Since the exact form of the $\tilde{K}^{-1}$ is not known in this (unphysical) region we cut it off with a simple form factor replacing $\tilde{K}^{-1} \to (1 + e^{-(\sigma - \sigma_0)/M_\pi^2})\tilde{K}^{-1}, \sigma_0 = 2M_\pi^2$. We have tested other functional forms and values of σ_0 and $\boldsymbol{p}_{\max}$, finding no relevant effect on the extracted observables. For further details on cutoff effects in the context of three-body systems see [44, 71, 76].

Results and discussion—The two-body finite-volume spectra consist of three energy eigenvalues located below the first inelastic threshold considering that two pions need to have one unit of momentum for the T_1^-. In the three-body spectra, we restrict ourselves to the analysis of the ground states and the first excited state for larger-volume ensembles as shown in Fig. 2. While qualitatively also higher levels seem to be predicted by the approach, their quantitative study requires a larger set of lattice operators as well as a formalism update with more free parameters due to the close proximity of the next excited state of the ω meson, the $\omega(1420)$.

With respect to these data, the method GEN yields best fits with $\chi^2_{\text{d.o.f.}}(\text{GEN}, 305) = 1.3$, $\chi^2_{\text{d.o.f.}}(\text{GEN}, 208) = 1.6$ including cross-correlations. For more details of the fit results and the obtained parameters, see [59]. Global EFT2 fits yield $\chi^2_{\text{d.o.f.}}(\text{EFT2}, 305/208) = 3.2$. Provided the precision level of our data, it is noticeable that the EFT2 model is also excessively rigid. Furthermore the corresponding pole positions at the physical point exhibit discrepancies with the empirical data. The EFT4 fit provides a much better description of the finite-volume spectrum $\chi^2_{\text{d.o.f.}}(\text{EFT4}, 208/305) = 2.3$ for $g_{\text{EFT4}} = 5.96(17)$, $\delta_{\text{EFT4}} = 38.8(6.9)\,\text{MeV}$, $M_{V,\text{EFT4}} = 737(12)\,\text{MeV}$, $a_{\text{EFT4}} = 0.96(14)\,\text{GeV}^{-1}$, which are, indeed, quite close to the phenomenological values [3, 86]. We consider EFT4 as our main result, with GEN and EFT2 results providing a measure for systematic uncertainties.

The resulting ω-pole positions using the IVU formalism Eq. (3) with respect to the discussed methods are shown in Fig. 3 (for ρ see [59]). In both cases and for each pion mass, we observe 1σ agreement between all methods regarding the real part of the pole position, while the imaginary part agrees on the level of 2σ. For the heavier
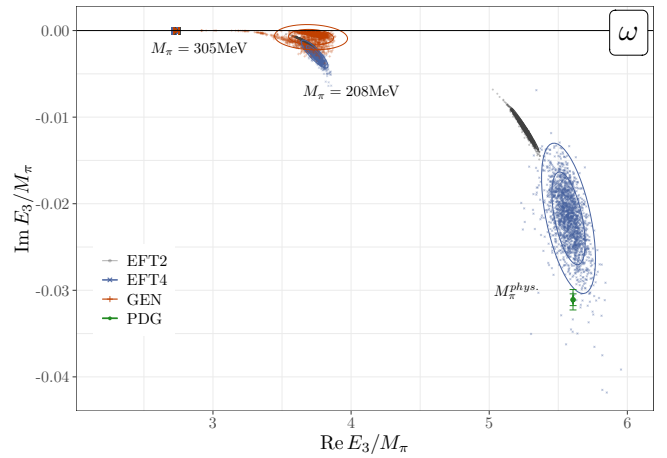

FIG. 3. Pole positions of the ω meson at varying pion mass from the IVU approach using generic and effective field theory form of the two- and three-body force. The points are the pole position for each bootstrap sample, whereas the ellipses represent the one- and two-sigma confidence levels. Parameters are fixed by fitting to the available lattice results at $M_\pi = 208$ and $M_\pi = 305\,\text{MeV}$ allowing one to extrapolate to the physical point. Particle Data Group (PDG) results are quoted by the green error bars for comparison [87–89].

pion mass value, the ω meson is indeed a bound state (binding energy $\sim 80\,\text{MeV}$). We note that the GEN results for the ω have to be taken with caution since for each pion mass only two volumes are available for the ω channel with one data point in the relevant energy region, leading possibly to a residual mass and width dependence. Because EFT results connect different pion masses this is not an issue there. The EFT2 pole positions are narrowed to a small region being parametrized only by two parameters (g, δ). The EFT4 agrees much better with the lattice results on the level of the finite-volume spectra as well as the corresponding GEN pole positions. Extrapolated to the physical pion mass it agrees astonishingly well ($< 1\sigma$) with the phenomenological ρ- and ω- masses [87] and within 2σ also with their widths. The numerical results in physical units read as

$$\sqrt{s_\rho} = [748.9(10.0) - i\,63.5(1.8)]\,\text{MeV}, \qquad (4)$$
$$\sqrt{s_\omega} = [778.0(11.2) - i\,3.0(5)] \qquad \text{MeV}, \qquad (5)$$

implying for instance also an $\omega - \rho$ mass difference of $29(15)\,\text{MeV}$, which agrees surprisingly well with the result obtained in [90]. The small deviation from the empirical value could be mitigated by taking into account the fact that in some cases too small volumes (see Table I) could give non-negligible exponential effects and discretization errors.

Conclusions—We have reported the first-ever lattice QCD estimates of the ω meson mass and width. One challenge in this calculation consists in particular in the

precise estimation of finite-volume spectra from lattice QCD. In resolving the complete low-lying spectrum of states, multihadron operators prove to be essential [33]. The three-particle operators we use (see [59]) require a significant computational effort to compute all the relevant fermion contractions, a task which has only recently become feasible due to advances in algorithms, methods, and computational power. Another challenge concerns the formalism development to not only map the finite-volume results to the infinite-volume transition amplitudes but to also establish a reliable connection to the pertinent effective field theories, allowing us to perform the so far unprecedented chiral extrapolation of three-body resonance parameters to the physical point. The final results show a good agreement of this theoretical multistep procedure with the empirical values [87] regarding the mass of both ρ and ω mesons. The ω width turns out slightly smaller than the experimental value, but still agrees within 2σ uncertainties. We refer here to an ongoing discussion on the current empirical values [91–95].

The presented study marks a new milestone in hadron spectroscopy from lattice QCD, paving the way toward understanding more complex systems. For closer to physical pion mass lattice setups the kinematic window to study resonance properties shrinks due to the proximity of the next inelastic thresholds (e.g., 5π). Thus, it may be advantageous to use more stable and widely available results at unphysical pion mass values and extrapolate to the physical point by making use of robust EFT methodology. While standard in two-body studies, such a treatment of resonant three-body systems has not yet been available. Future steps include the assessment of discretization errors as well as the inclusion of larger volumes to reduce the systematic uncertainties further. Applications toward the Roper resonance and T_{cc} are also planned.

———————————

* haobo@stu.pku.edu.cn
† maxim.mai@faculty.unibe.ch
‡ garofalo@hiskp.uni-bonn.de
§ meissner@hiskp.uni-bonn.de
¶ liuchuan@pku.edu.cn
** liuming@impcas.ac.cn
†† urbach@hiskp.uni-bonn.de

[1] J. J. Sakurai, Theory of strong interactions, Annals Phys. **11**, 1 (1960).

[2] R. P. Feynman, *Photon-hadron interactions* (W.A. Benjamin, Reading, MA, 1972).

[3] U.-G. Meißner, N. Kaiser, A. Wirzba, and W. Weise, Skyrmions With ρ and ω Mesons as Dynamical Gauge Bosons, Phys. Rev. Lett. **57**, 1676 (1986).

[4] N. Kaiser and W. Weise, Sizes of the nucleon, Phys. Rev. C **110**, 015202 (2024), arXiv:2404.11292 [nucl-th].

[5] K. Erkelenz, Current status of the relativistic two nucleon one boson exchange potential, Phys. Rept. **13**, 191 (1974).

[6] G. Brown and A. Jackson, *The nucleon-nucleon interaction* (North-Holland, Amsterdam, 1976).

[7] L. M. Barkov *et al.*, Electromagnetic Pion Form-Factor in the Timelike Region, Nucl. Phys. B **256**, 365 (1985).

[8] H. B. O'Connell, B. C. Pearce, A. W. Thomas, and A. G. Williams, $\rho - \omega$ mixing, vector meson dominance and the pion form-factor, Prog. Part. Nucl. Phys. **39**, 201 (1997), arXiv:hep-ph/9501251.

[9] C. McNeile *et al.* (Fermilab Lattice, HPQCD, MILC), Progress report on computing the disconnected QCD and the QCD plus QED hadronic contributions to the muon's anomalous magnetic moment., PoS **LATTICE2021**, 039 (2022), arXiv:2112.11339 [hep-lat].

[10] M. Hoferichter, G. Colangelo, B.-L. Hoid, B. Kubis,

J. R. de Elvira, D. Schuh, D. Stamen, and P. Stoffer, Phenomenological Estimate of Isospin Breaking in Hadronic Vacuum Polarization, Phys. Rev. Lett. **131**, 161905 (2023), arXiv:2307.02532 [hep-ph].

[11] P. Stoffer, G. Colangelo, and M. Hoferichter, Puzzles in the hadronic contributions to the muon anomalous magnetic moment, JINST **18** (10), C10021, arXiv:2308.04217 [hep-ph].

[12] M. Hippert, J. Setford, H. Tan, D. Curtin, J. Noronha-Hostler, and N. Yunes, Mirror neutron stars, Phys. Rev. D **106**, 035025 (2022), arXiv:2103.01965 [astro-ph.HE].

[13] M. Hippert, E. Dillingham, H. Tan, D. Curtin, J. Noronha-Hostler, and N. Yunes, Dark matter or regular matter in neutron stars? How to tell the difference from the coalescence of compact objects, Phys. Rev. D **107**, 115028 (2023), arXiv:2211.08590 [astro-ph.HE].

[14] M. G. Alford and R. L. Jaffe, Insight into the scalar mesons from a lattice calculation, Nucl. Phys. B **578**, 367 (2000), arXiv:hep-lat/0001023.

[15] S. Prelovsek, T. Draper, C. B. Lang, M. Limmer, K.-F. Liu, N. Mathur, and D. Mohler, Lattice study of light scalar tetraquarks with $I = 0, 2, 1/2, 3/2$: Are σ and κ tetraquarks?, Phys. Rev. D **82**, 094507 (2010), arXiv:1005.0948 [hep-lat].

[16] Z. Fu, Preliminary lattice study of σ meson decay width, JHEP **07**, 142, arXiv:1202.5834 [hep-lat].

[17] Z. Fu, Lattice QCD study of the s-wave $\pi\pi$ scattering lengths in the I=0 and 2 channels, Phys. Rev. D **87**, 074501 (2013), arXiv:1303.0517 [hep-lat].

[18] R. A. Briceno, J. J. Dudek, R. G. Edwards, and D. J. Wilson, Isoscalar $\pi\pi$ scattering and the σ meson resonance from QCD, Phys. Rev. Lett. **118**, 022002 (2017), arXiv:1607.05900 [hep-ph].

[19] M. Döring, B. Hu, and M. Mai, Chiral Extrapolation of the Sigma Resonance, Phys. Lett. B **782**, 785 (2018), arXiv:1610.10070 [hep-lat].

[20] L. Liu *et al.*, Isospin-0 $\pi\pi$ s-wave scattering length from twisted mass lattice QCD, Phys. Rev. D **96**, 054516 (2017), arXiv:1612.02061 [hep-lat].

[21] Z. Fu and X. Chen, $I = 0$ $\pi\pi$ s-wave scattering length from lattice QCD, Phys. Rev. D **98**, 014514 (2018), arXiv:1712.02219 [hep-lat].

[22] D. Guo, A. Alexandru, R. Molina, M. Mai, and M. Döring, Extraction of isoscalar $\pi\pi$ phase-shifts from lattice QCD, Phys. Rev. D **98**, 014507 (2018), arXiv:1803.02897 [hep-lat].

[23] R. A. Briceno, J. J. Dudek, R. G. Edwards, and D. J. Wilson, Isoscalar $\pi\pi$, $K\overline{K}$, $\eta\eta$ scattering and the σ, f_0, f_2 mesons from QCD, Phys. Rev. D **97**, 054513 (2018), arXiv:1708.06667 [hep-lat].

[24] D. Guo, A. Alexandru, R. Molina, and M. Döring, Rho resonance parameters from lattice QCD, Phys. Rev. D **94**, 034501 (2016), arXiv:1605.03993 [hep-lat].

[25] S. Aoki *et al.* (CP-PACS), Lattice QCD Calculation of the rho Meson Decay Width, Phys. Rev. D **76**, 094506 (2007), arXiv:0708.3705 [hep-lat].

[26] G. S. Bali, S. Collins, A. Cox, G. Donald, M. Göckeler, C. B. Lang, and A. Schäfer (RQCD), ρ and K^* resonances on the lattice at nearly physical quark masses and $N_f = 2$, Phys. Rev. D **93**, 054509 (2016), arXiv:1512.08678 [hep-lat].

[27] C. B. Lang, D. Mohler, S. Prelovsek, and M. Vidmar, Coupled channel analysis of the rho meson decay in lattice QCD, Phys. Rev. D **84**, 054503 (2011), [Erratum:

Phys.Rev.D 89, 059903 (2014)], arXiv:1105.5636 [hep-lat].

[28] X. Feng, K. Jansen, and D. B. Renner, Resonance Parameters of the rho-Meson from Lattice QCD, Phys. Rev. D **83**, 094505 (2011), arXiv:1011.5288 [hep-lat].

[29] M. Fischer, B. Kostrzewa, M. Mai, M. Petschlies, F. Pittler, M. Ueding, C. Urbach, and M. Werner (Extended Twisted Mass, ETM), The ρ-resonance from $N_f = 2$ lattice QCD including the physical pion mass, Phys. Lett. B **819**, 136449 (2021), arXiv:2006.13805 [hep-lat].

[30] C. Pelissier and A. Alexandru, Resonance parameters of the rho-meson from asymmetrical lattices, Phys. Rev. D **87**, 014503 (2013), arXiv:1211.0092 [hep-lat].

[31] F. Erben, J. R. Green, D. Mohler, and H. Wittig, Rho resonance, timelike pion form factor, and implications for lattice studies of the hadronic vacuum polarization, Phys. Rev. D **101**, 054504 (2020), arXiv:1910.01083 [hep-lat].

[32] S. Aoki *et al.* (CS), ρ Meson Decay in 2+1 Flavor Lattice QCD, Phys. Rev. D **84**, 094505 (2011), arXiv:1106.5365 [hep-lat].

[33] D. J. Wilson, R. A. Briceno, J. J. Dudek, R. G. Edwards, and C. E. Thomas, Coupled $\pi\pi$, $K\overline{K}$ scattering in P-wave and the ρ resonance from lattice QCD, Phys. Rev. D **92**, 094502 (2015), arXiv:1507.02599 [hep-ph].

[34] J. Bulava, B. Fahy, B. Hörz, K. J. Juge, C. Morningstar, and C. H. Wong, $I = 1$ and $I = 2$ $\pi - \pi$ scattering phase shifts from $N_f = 2 + 1$ lattice QCD, Nucl. Phys. B **910**, 842 (2016), arXiv:1604.05593 [hep-lat].

[35] Z. Fu and L. Wang, Studying the ρ resonance parameters with staggered fermions, Phys. Rev. D **94**, 034505 (2016), arXiv:1608.07478 [hep-lat].

[36] W. Sun, A. Alexandru, Y. Chen, T. Draper, Z. Liu, and Y.-B. Yang (χQCD), Anatomy of the ρ resonance from lattice QCD at the physical point, Chin. Phys. C **42**, 063102 (2018), arXiv:1507.02541 [hep-ph].

[37] C. Alexandrou, L. Leskovec, S. Meinel, J. Negele, S. Paul, M. Petschlies, A. Pochinsky, G. Rendon, and S. Syritsyn, P-wave $\pi\pi$ scattering and the ρ resonance from lattice QCD, Phys. Rev. D **96**, 034525 (2017), arXiv:1704.05439 [hep-lat].

[38] C. Andersen, J. Bulava, B. Hörz, and C. Morningstar, The $I = 1$ pion-pion scattering amplitude and timelike pion form factor from $N_f = 2 + 1$ lattice QCD, Nucl. Phys. B **939**, 145 (2019), arXiv:1808.05007 [hep-lat].

[39] Y. Akahoshi, S. Aoki, and T. Doi, Emergence of the ρ resonance from the HAL QCD potential in lattice QCD, Phys. Rev. D **104**, 054510 (2021), arXiv:2106.08175 [hep-lat].

[40] M. Werner *et al.* (Extended Twisted Mass), Hadron-Hadron Interactions from $N_f = 2 + 1 + 1$ Lattice QCD: The ρ-resonance, Eur. Phys. J. A **56**, 61 (2020), arXiv:1907.01237 [hep-lat].

[41] P. Boyle, F. Erben, V. Gülpers, M. T. Hansen, F. Joswig, N. P. Lachini, M. Marshall, and A. Portelli, Light and strange vector resonances from lattice QCD at physical quark masses (2024), arXiv:2406.19194 [hep-lat].

[42] P. Boyle, F. Erben, V. Gülpers, M. T. Hansen, F. Joswig, N. P. Lachini, M. Marshall, and A. Portelli, Physical-mass calculation of $\rho(770)$ and $K^*(892)$ resonance parameters via $\pi\pi$ and $K\pi$ scattering amplitudes from lattice QCD (2024), arXiv:2406.19193 [hep-lat].

[43] M. Mai, U.-G. Meißner, and C. Urbach, Towards a theory of hadron resonances, Phys. Rept. **1001**, 1 (2023), arXiv:2206.01477 [hep-ph].

[44] M. Mai and M. Döring, Finite-Volume Spectrum of $\pi^+\pi^+$ and $\pi^+\pi^+\pi^+$ Systems, Phys. Rev. Lett. **122**, 062503 (2019), arXiv:1807.04746 [hep-lat].

[45] T. D. Blanton, F. Romero-López, and S. R. Sharpe, $I = 3$ Three-Pion Scattering Amplitude from Lattice QCD, Phys. Rev. Lett. **124**, 032001 (2020), arXiv:1909.02973 [hep-lat].

[46] C. Culver, M. Mai, R. Brett, A. Alexandru, and M. Döring, Three pion spectrum in the $I = 3$ channel from lattice QCD, Phys. Rev. D **101**, 114507 (2020), arXiv:1911.09047 [hep-lat].

[47] M. T. Hansen, R. A. Briceño, R. G. Edwards, C. E. Thomas, and D. J. Wilson (Hadron Spectrum), Energy-Dependent $\pi^+\pi^+\pi^+$ Scattering Amplitude from QCD, Phys. Rev. Lett. **126**, 012001 (2021), arXiv:2009.04931 [hep-lat].

[48] M. Fischer, B. Kostrzewa, L. Liu, F. Romero-López, M. Ueding, and C. Urbach, Scattering of two and three physical pions at maximal isospin from lattice QCD, Eur. Phys. J. C **81**, 436 (2021), arXiv:2008.03035 [hep-lat].

[49] A. Alexandru, R. Brett, C. Culver, M. Döring, D. Guo, F. X. Lee, and M. Mai, Finite-volume energy spectrum of the $K^-K^-K^-$ system, Phys. Rev. D **102**, 114523 (2020), arXiv:2009.12358 [hep-lat].

[50] Z. T. Draper, A. D. Hanlon, B. Hörz, C. Morningstar, F. Romero-López, and S. R. Sharpe, Interactions of πK, $\pi\pi K$ and $KK\pi$ systems at maximal isospin from lattice QCD, JHEP **05**, 137, arXiv:2302.13587 [hep-lat].

[51] M. Mai, A. Alexandru, R. Brett, C. Culver, M. Döring, F. X. Lee, and D. Sadasivan (GWQCD), Three-Body Dynamics of the $a_1(1260)$ Resonance from Lattice QCD, Phys. Rev. Lett. **127**, 222001 (2021), arXiv:2107.03973 [hep-lat].

[52] M. T. Hansen and S. R. Sharpe, Lattice QCD and Three-particle Decays of Resonances, Ann. Rev. Nucl. Part. Sci. **69**, 65 (2019), arXiv:1901.00483 [hep-lat].

[53] M. Mai, M. Döring, and A. Rusetsky, Multi-particle systems on the lattice and chiral extrapolations: a brief review, Eur. Phys. J. ST **230**, 1623 (2021), arXiv:2103.00577 [hep-lat].

[54] M. Mai and M. Döring, Three-body Unitarity in the Finite Volume, Eur. Phys. J. A **53**, 240 (2017), arXiv:1709.08222 [hep-lat].

[55] M. Gell-Mann, D. Sharp, and W. G. Wagner, Decay rates of neutral mesons, Phys. Rev. Lett. **8**, 261 (1962).

[56] U.-G. Meißner, Low-Energy Hadron Physics from Effective Chiral Lagrangians with Vector Mesons, Phys. Rept. **161**, 213 (1988).

[57] Z.-C. Hu, B.-L. Hu, J.-H. Wang, M. Gong, G. Liu, L. Liu, P. Sun, W. Sun, W. Wang, Y.-B. Yang, and D.-J. Zhao (CLQCD Collaboration), Quark masses and low-energy constants in the continuum from the tadpole-improved clover ensembles, Phys. Rev. D **109**, 054507 (2024).

[58] H. Yan, Operator construction (OpTion), https://github.com/wittscien/OpTion (2024).

[59] See Supplemental Material for the table of operators, topologies of the contraction diagrams, the details of the extraction of the finite-volume spectra, and the details on the FVU fit results, which includes Refs. [60, 61, 62] of PDG results for comparison.

[60] R. Garcia-Martin, R. Kaminski, J. R. Pelaez, and J. Ruiz de Elvira, Precise determination of the $f_0(600)$ and $f_0(980)$ pole parameters from a dispersive data analysis, Phys. Rev. Lett. **107**, 072001 (2011), arXiv:1107.1635 [hep-ph].

[61] J. R. Pelaez, Light scalars as tetraquarks or two-meson states from large N_c and unitarized chiral perturbation theory, Mod. Phys. Lett. A **19**, 2879 (2004), arXiv:hep-ph/0411107.

[62] G. Colangelo, J. Gasser, and H. Leutwyler, $\pi\pi$ scattering, Nucl. Phys. B **603**, 125 (2001), arXiv:hep-ph/0103088.

[63] C. Michael and I. Teasdale, Extracting Glueball Masses From Lattice QCD, Nucl. Phys. B **215**, 433 (1983).

[64] M. Luscher and U. Wolff, How to Calculate the Elastic Scattering Matrix in Two-dimensional Quantum Field Theories by Numerical Simulation, Nucl. Phys. B **339**, 222 (1990).

[65] B. Blossier, M. Della Morte, G. von Hippel, T. Mendes, and R. Sommer, On the generalized eigenvalue method for energies and matrix elements in lattice field theory, JHEP **04**, 094, arXiv:0902.1265 [hep-lat].

[66] M. Fischer, B. Kostrzewa, J. Ostmeyer, K. Ottnad, M. Ueding, and C. Urbach, On the generalised eigenvalue method and its relation to Prony and generalised pencil of function methods, Eur. Phys. J. A **56**, 206 (2020), arXiv:2004.10472 [hep-lat].

[67] M. Peardon, J. Bulava, J. Foley, C. Morningstar, J. Dudek, R. G. Edwards, B. Joó, H.-W. Lin, D. G. Richards, and K. J. Juge (Hadron Spectrum Collaboration), Novel quark-field creation operator construction for hadronic physics in lattice QCD, Phys. Rev. D **80**, 054506 (2009).

[68] M. Mai, M. Döring, C. Culver, and A. Alexandru, Three-body unitarity versus finite-volume $\pi^+\pi^+\pi^+$ spectrum from lattice QCD, Phys. Rev. D **101**, 054510 (2020), arXiv:1909.05749 [hep-lat].

[69] R. Brett, C. Culver, M. Mai, A. Alexandru, M. Döring, and F. X. Lee, Three-body interactions from the finite-volume QCD spectrum, Phys. Rev. D **104**, 014501 (2021), arXiv:2101.06144 [hep-lat].

[70] M. Garofalo, M. Mai, F. Romero-López, A. Rusetsky, and C. Urbach, Three-body resonances in the φ^4 theory, JHEP **02**, 252, arXiv:2211.05605 [hep-lat].

[71] Y. Feng, F. Gil, M. Döring, R. Molina, M. Mai, V. Shastry, and A. Szczepaniak, A unitary coupled-channel three-body amplitude with pions and kaons, (2024), arXiv:2407.08721 [nucl-th].

[72] A. W. Jackura, S. M. Dawid, C. Fernández-Ramírez, V. Mathieu, M. Mikhasenko, A. Pilloni, S. R. Sharpe, and A. P. Szczepaniak, Equivalence of three-particle scattering formalisms, Phys. Rev. D **100**, 034508 (2019), arXiv:1905.12007 [hep-ph].

[73] M. Göckeler, R. Horsley, M. Lage, U.-G. Meißner, P. E. L. Rakow, A. Rusetsky, G. Schierholz, and J. M. Zanotti, Scattering phases for meson and baryon resonances on general moving-frame lattices, Phys. Rev. D **86**, 094513 (2012), arXiv:1206.4141 [hep-lat].

[74] M. Lüscher, Two particle states on a torus and their relation to the scattering matrix, Nucl. Phys. B **354**, 531 (1991).

[75] S. U. Chung, SPIN FORMALISMS 10.5170/CERN-1971-008 (1971).

[76] D. Sadasivan, M. Mai, H. Akdag, and M. Döring, Dalitz plots and lineshape of $a_1(1260)$ from a relativistic three-body unitary approach, Phys. Rev. D **101**, 094018 (2020), [Erratum: Phys.Rev.D 103, 019901 (2021)], arXiv:2002.12431 [nucl-th].

[77] M. Mai, C. Culver, A. Alexandru, M. Döring, and

F. X. Lee, Cross-channel study of pion scattering from lattice QCD, Phys. Rev. D **100**, 114514 (2019), arXiv:1908.01847 [hep-lat].

[78] Riazuddin and Fayyazuddin, Algebra of current components and decay widths of rho and K^* mesons, Phys. Rev. **147**, 1071 (1966).

[79] K. Kawarabayashi and M. Suzuki, Partially conserved axial vector current and the decays of vector mesons, Phys. Rev. Lett. **16**, 255 (1966).

[80] J. Gasser and H. Leutwyler, Chiral Perturbation Theory to One Loop, Annals Phys. **158**, 142 (1984).

[81] P. C. Bruns and U.-G. Meißner, Infrared regularization for spin-1 fields, Eur. Phys. J. C **40**, 97 (2005), arXiv:hep-ph/0411223.

[82] K. Yu, Y. Li, J.-J. Wu, D. B. Leinweber, and A. W. Thomas, Study of the pion-mass dependence of ρ-meson properties in lattice QCD, Phys. Rev. D **109**, 034505 (2024), arXiv:2311.03903 [hep-lat].

[83] M. Mai, B. Hu, M. Döring, A. Pilloni, and A. Szczepaniak, Three-body Unitarity with Isobars Revisited, Eur. Phys. J. A **53**, 177 (2017), arXiv:1706.06118 [nucl-th].

[84] D. Sadasivan, A. Alexandru, H. Akdag, F. Amorim, R. Brett, C. Culver, M. Döring, F. X. Lee, and M. Mai, Pole position of the a1(1260) resonance in a three-body unitary framework, Phys. Rev. D **105**, 054020 (2022), arXiv:2112.03355 [hep-ph].

[85] J. H. Hetherington and L. H. Schick, Exact Multiple-Scattering Analysis of Low-Energy Elastic K–d Scattering with Separable Potentials, Phys. Rev. **137**, B935 (1965).

[86] M. Dax, T. Isken, and B. Kubis, Quark-mass dependence in $\omega \to 3\pi$ decays, Eur. Phys. J. C **78**, 859 (2018), arXiv:1808.08957 [hep-ph].

[87] R. L. Workman *et al.* (Particle Data Group), Review of Particle Physics, PTEP **2022**, 083C01 (2022).

[88] R. R. Akhmetshin *et al.* (CMD-2), Reanalysis of hadronic cross-section measurements at CMD-2, Phys. Lett. B **578**, 285 (2004), arXiv:hep-ex/0308008.

[89] M. N. Achasov *et al.*, Study of the process $e^+e^- \to \pi^+\pi^-\pi^0$ in the energy region $\sqrt{s}$ below 0.98 GeV, Phys. Rev. D **68**, 052006 (2003), arXiv:hep-ex/0305049.

[90] C. McNeile, C. Michael, and C. Urbach (ETM), The omega-rho meson mass splitting and mixing from lattice QCD, Phys. Lett. B **674**, 286 (2009), arXiv:0902.3897 [hep-lat].

[91] M. Hoferichter, B.-L. Hoid, B. Kubis, and D. Schuh, Isospin-breaking effects in the three-pion contribution to hadronic vacuum polarization, JHEP **08**, 208, arXiv:2307.02546 [hep-ph].

[92] M. Hoferichter, B.-L. Hoid, and B. Kubis, Three-pion contribution to hadronic vacuum polarization, JHEP **08**, 137, arXiv:1907.01556 [hep-ph].

[93] B.-L. Hoid, M. Hoferichter, and B. Kubis, Hadronic vacuum polarization and vector-meson resonance parameters from $e^+e^- \to \pi^0\gamma$, Eur. Phys. J. C **80**, 988 (2020), arXiv:2007.12696 [hep-ph].

[94] G. Colangelo, M. Hoferichter, B. Kubis, and P. Stoffer, Isospin-breaking effects in the two-pion contribution to hadronic vacuum polarization, JHEP **10**, 032, arXiv:2208.08993 [hep-ph].

[95] G. Colangelo, M. Hoferichter, and P. Stoffer, Two-pion contribution to hadronic vacuum polarization, JHEP **02**, 006, arXiv:1810.00007 [hep-ph].

[96] M. Clark, R. Babich, K. Barros, R. Brower, and C. Rebbi, Solving lattice qcd systems of equations using mixed precision solvers on gpus, Computer Physics Communications **181**, 1517 (2010).

[97] R. Babich, M. A. Clark, B. Joó, G. Shi, R. C. Brower, and S. Gottlieb, Scaling lattice qcd beyond 100 gpus, in *Proceedings of 2011 International Conference for High Performance Computing, Networking, Storage and Analysis*, SC '11 (2011).

[98] M. A. Clark, B. Joó, A. Strelchenko, M. Cheng, A. Gambhir, and R. C. Brower, Accelerating lattice QCD multigrid on gpus using fine-grained parallelization, in *Proceedings of the International Conference for High Performance Computing, Networking, Storage and Analysis*, SC '16 (2016).

[99] H. Yan, C. Liu, L. Liu, Y. Meng, and H. Xing, Pion mass dependence in $D\pi$ scattering and the $D_0^*(2300)$ resonance from lattice QCD (2024), arXiv:2404.13479 [hep-lat].

SUPPLEMENTAL MATERIAL

1. Table of operators

Each operator used in this work is a linear combination of quark bilinear or the product of bilinears. First, we construct the operators in the flavor space. Let $\rho_i^+/\pi^+ = \bar{d}\gamma_{i/5}u, [\rho/\pi]^u = \bar{u}\gamma_{i/5}d$, *etc.* For $I = 1$ $\pi\pi$ channel, the following flavor structure is used:

$$
\begin{cases}
|\rho\rangle & = -\rho^+, \\
|\pi\pi\rangle & = \frac{1}{2}\left[-\pi^+\pi^u + \pi^+\pi^d + \pi^u\pi^+ - \pi^d\pi^+\right],
\end{cases}
\tag{S1}
$$

where $|\rho\rangle$ and $|\pi\pi\rangle$ are one-body and two-body operators, respectively.

For $I = 0$ $\pi\pi\pi$ channel, the following structure of bilinears is designed to enforce the isoscalar projection

$$
\begin{cases}
|\omega\rangle & = \frac{1}{\sqrt{2}}(\omega^u + \omega^d), \\
|\rho\pi\rangle & = -\frac{1}{\sqrt{3}}\left[\rho^+\pi^- + \rho^-\pi^+ + \frac{1}{2}[\rho^u\pi^u - \rho^u\pi^d - \rho^d\pi^u + \rho^d\pi^d]\right], \\
|\pi\pi\pi\rangle & = \frac{1}{\sqrt{12}}\left[-\pi^+\pi^u\pi^- + \pi^+\pi^d\pi^- + \pi^u\pi^+\pi^- - \pi^d\pi^+\pi^- + \pi^+\pi^-\pi^u - \pi^+\pi^-\pi^d \right. \\
& \quad \left. -\pi^-\pi^+\pi^u + \pi^-\pi^+\pi^d - \pi^u\pi^-\pi^+ + \pi^d\pi^-\pi^+ + \pi^-\pi^u\pi^+ - \pi^-\pi^d\pi^+\right],
\end{cases}
\tag{S2}
$$

The operator set includes all one-, two-, and three-body operators to overlap with the dynamical channels in this study.

Second, the two-body operators are further projected onto the T_1^- irrep in the momentum space to detect the P-wave. With `OpTion` [58], the explicit forms of the operators are printed. For convenience, the operators are represented as

$$
\begin{cases}
O_{\text{one}} = \sum_i \eta_i \omega_{\mu_i}(0), \\
O_{\text{two}} = \sum_i \eta_i \rho_{\mu_i}(\vec{p}_i)\pi(-\vec{p}_i), \\
O_{\text{three}} = \sum_i \eta_i \pi_{\mu_i}(\vec{p}_{i1})\pi_{\mu_i}(\vec{p}_{i2})\pi(-\vec{p}_{i1} - \vec{p}_{i2}),
\end{cases}
\tag{S3}
$$

and are uniquely identified by the parameters η_i, μ_i and $\vec{p}_i$. $\mu_i \in \{0, 5, x, y, z\}$ is the Cartesian gamma matrices and corresponds to $\gamma_0, \gamma_5, \gamma_x, \gamma_y, \gamma_z$. $\vec{p}_i$ is the momenta for each meson. For convenience, the parameters are denoted by

$$
\eta_{\mu_i}^{\alpha_{i1}(;\alpha_{i2})},
\tag{S4}
$$

where α_i one-to-one corresponds to the momentum vector. One direction notation in α_i means one unit of momentum in that direction. For example, $\alpha = yz \to \vec{p} = [011]$, $\alpha = -2x \to \vec{p} = [-200]$, *etc.* The space projection coefficients are shown in Tab. S1.

channel	type	operator
$\pi\pi$	one	$(+1)_z^0$
	two	$(+1)_5^0$
		$(+1)_5^x, (+1)_5^{-x}, (+1)_5^y, (+1)_5^{-y}, (+1)_5^z, (+1)_5^{-z}$
$\pi\pi\pi$	one	$(+1)_z^0$
	two	$(-1)_x^{-y}, (+1)_x^y, (+1)_y^{-x}, (-1)_y^x$
		$(-1)_x^{xy}, (+1)_y^{xy}, (+1)_x^{x,-y}, (+1)_y^{x,-y}, (-1)_x^{-x,y}, (-1)_y^{-x,y}, (+1)_x^{-x,-y}, (-1)_y^{-x,-y}$
	three	$(+1)_5^{xy;-y}, (-1)_5^{x,-y;y}, (-1)_5^{-x,y;-y}, (+1)_5^{-x,-y;y}, (-1)_5^{xy;-x}, (+1)_5^{-x,y;x}, (+1)_5^{x,-y;-x}, (-1)_5^{-x,-y;x}$

TABLE S1. Operators used to interpolate the $\pi\pi$ and $\pi\pi\pi$ system. Each irrep contains both one-meson type, two-meson, and possible three-meson type operators. The symbols $\eta_{\mu_i}^{\alpha_{i1}(;\alpha_{i2})}$ are defined in the context. The overall constants are ignored.

Non-local operators with covariant derivatives are tested. The resulting spectra do not lead to noticeable change and as a result, this kind of operators are disposed out of the operator set.

2. Topologies of the contraction diagrams

After projecting to isospin $I = 0$, only certain topologies remain. The topologies of $\pi\pi\pi \to \pi\pi\pi$ are illustrated in the main text. The schematics of other diagrams including the three-pion operators, *i.e.*, $\pi\pi\pi \to \rho\pi$ and $\pi\pi\pi \to \omega$, are shown in Fig. S1.
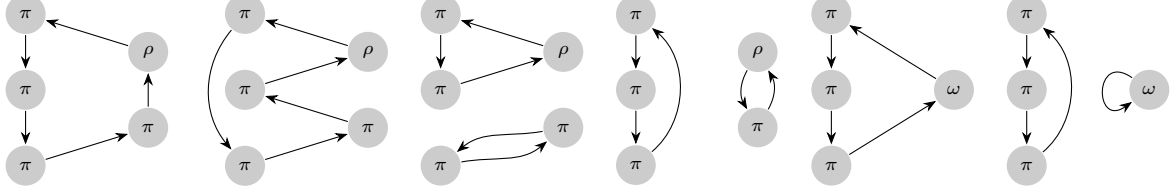

FIG. S1. Topologies of the diagrams for $\pi\pi\pi \to \rho\pi$ and $\pi\pi\pi \to \omega$.

Topologies in the two-pion and one-pion sectors are shown in Fig S2. The type of topologies is the same as those for $I = 0$ $\pi\pi$ scattering, with one of the π replaced by the ρ meson and the target resonance σ replaced by the ω.
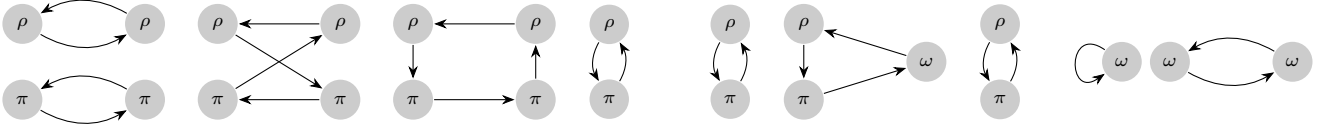

FIG. S2. Topologies of the diagrams for $\rho\pi \to \rho\pi$, $\rho\pi \to \omega$, and $\omega \to \omega$.

3. Spectra

In this section, we present the details of extracting finite-volume energy levels from the correlation matrices $C_{ij}(t)$. To determine the lowest levels, we solve the GEVP for each ensemble,

$$C(t)v_n(t, t_0) = \lambda_n(t, t_0)C(t_0)v_n(t, t_0),\tag{S5}$$

where $\lambda_n(t, t_0)$ are the eigenvalues corresponding to the eigenvectors $v_n(t, t_0)$. For the $\pi\pi$ channel, we use 3×3 matrices and for the $\pi\pi\pi$ channel, we use 4×4 matrices using the operators in Table S1. The choice of the reference time t_0 has a negligible impact on the resulting spectra.

The effective mass of the eigenvalues in the $\pi\pi$ and $\pi\pi\pi$ channel are shown in Figs. S3 and S3, respectively. The plots exhibit plateaus at large t. The thermal pollution in the $\pi\pi$ channel is eliminated by shifting the correlation matrices before solving GEVP. The thermal pollution in the $\pi\pi\pi$ channel is not evident with the current precision, and is, thus, ignored in the analysis.

The energy levels of the nth excited states are extracted by doing a two-state fit of $\lambda_n(t, t_0)$:

$$\lambda_n(t, t_0) = (1 - A_n)\,e^{-E_n(t-t_0)} + A_n\,e^{-E'_n(t-t_0)},\tag{S6}$$

where E_n is the nth energy level.

We inspected the dependence of the levels on the fitting range and chose the starting point $t_{\min}$ such that the fit yields a reasonable χ^2_{dof} and remains stable against changes in the fitting range. An example of this stability analysis for the ground state in the $\pi\pi\pi$ channel of ensemble F32P21 is shown in Fig. S5. Statistical uncertainties are estimated from 2000 Bootstrap samples.

4. Fit results

Details of the fit results for the GEN(305), GEN(208), EFT2(208/305) and EFT4(208/305) methods of parametrizing two- and three-body force. All values are estimated for the $\boldsymbol{p}_{\max} = (2\pi)/L(0, 1, 1)$ spectator momentum cutoff and
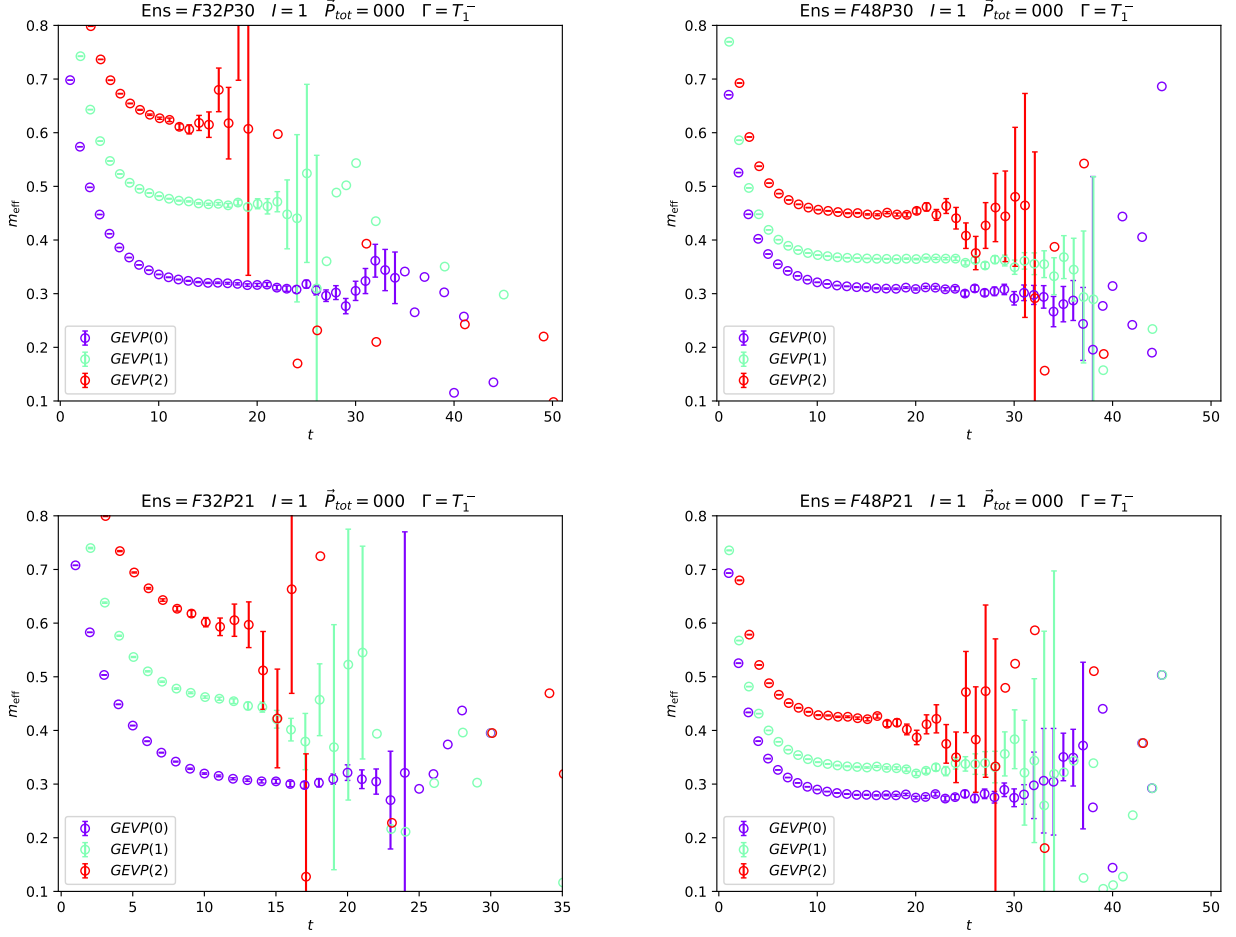
FIG. S3. Effective masses of the GEVP eigenvalues in the $I = 1\,\pi\pi$ channel.

left-hand cutoff form-factor $\tilde{K}^{-1} \to (1 + e^{-(\sigma-\sigma_0)/M_\pi^2})\tilde{K}^{-1}$. Statistical uncertainties are estimated from 2000 Bootstrap samples. For the EFT4 fit, we also estimated the systematic uncertainty from the exponential finite-volume effect by excluding energy levels from the F32P21 ensemble, which has the smallest $M_\pi L$. The difference in the fit parameters with and without this ensemble is reported as the second error. This uncertainty remains within or slightly above the statistical error, suggesting that the finite-volume effect does not significantly impact our fit. The distribution and covariances of the parameters of GEN and EFT fits are shown in the corner plots Fig. S6 and Fig. S7, respectively.

M_π/MeV	$\tilde{K}^{-1}$	c_{11}	χ^2_{dof}	Parameters
305	$a_0 + a_1\sigma$	$\frac{c_0}{s-M_\omega^2}$	1.25	$a_0 = -9556(597)\,\mathrm{MeV}^2,\ a_1 = 0.01393(94),\ c_0 = 5.7(4.2)\times10^6\,\mathrm{MeV}^2,\ M_\omega = 841.5(7.3)\,\mathrm{MeV}$
208	$a_0 + a_1\sigma$	$\frac{c_0}{s-M_\omega^2}$	1.57	$a_0 = -8068(718)\,\mathrm{MeV}^2,\ a_1 = 0.0130(14),\ c_0 = 2(17)\times10^6\,\mathrm{MeV}^2,\ M_\omega = 784(13)\,\mathrm{MeV}$
305/208	$\frac{\sigma - M_\rho^2}{2g^2}$	c_{11}^{EFT}	3.16	$g = 5.432(29),\ \delta = 36.2(6.7)\ \mathrm{MeV}$
	$\frac{\sigma - M_\rho^2(M_V,a)}{2g^2}$	c_{11}^{EFT}	2.29	$g = 5.960(167)[5],\ \delta = 38.8(6.9)[7.3]\ \mathrm{MeV},\ M_V = 737(12)[2]\ \mathrm{MeV},\ a = 0.00096(14)[4]\ \mathrm{MeV}^{-1}$

TABLE S2. Results for simultaneous 2/3-body fit.

The resulting ρ pole positions using the procedure described in Sec *Quantization conditions and resonance parameter* of the main text are shown in Fig. S8.
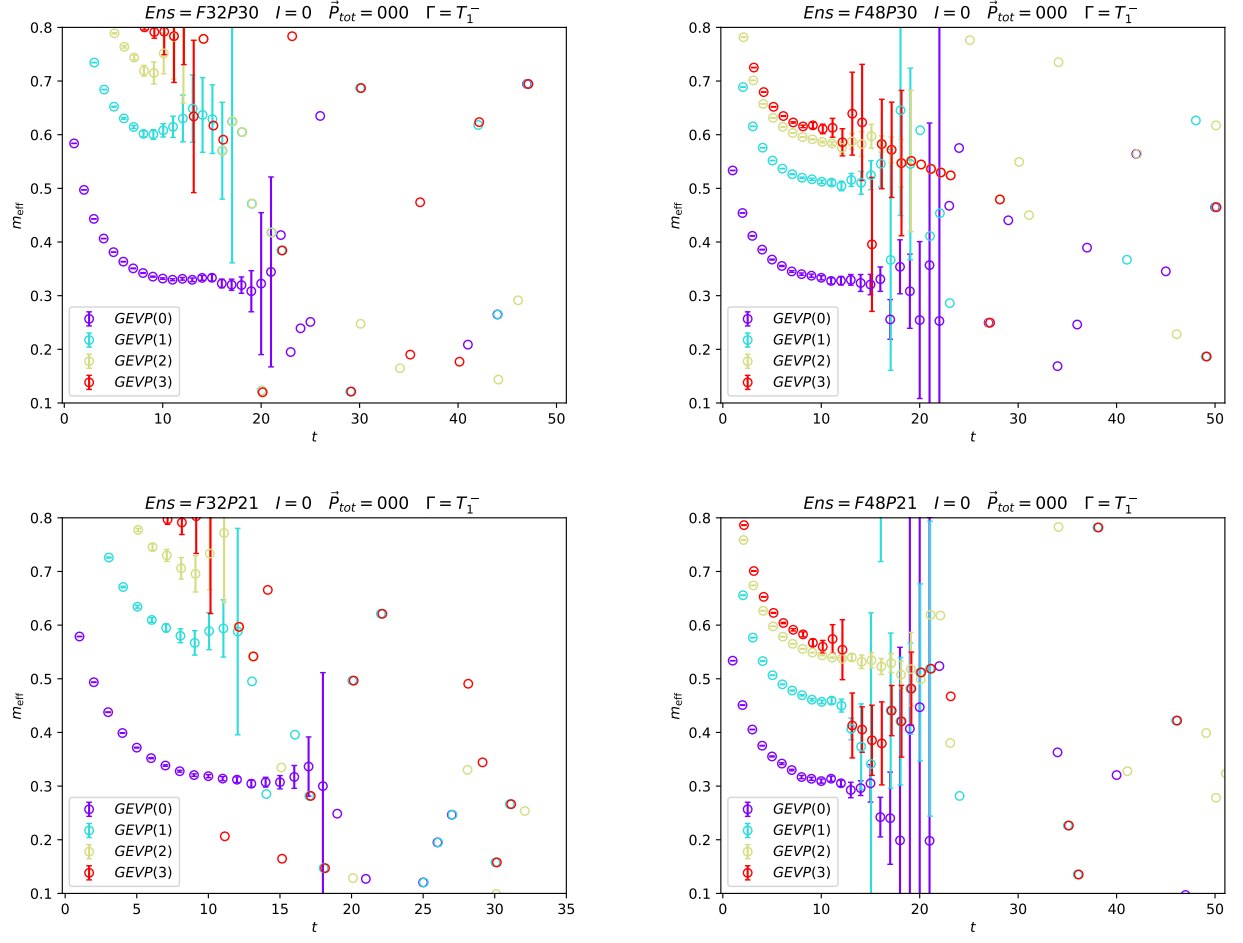
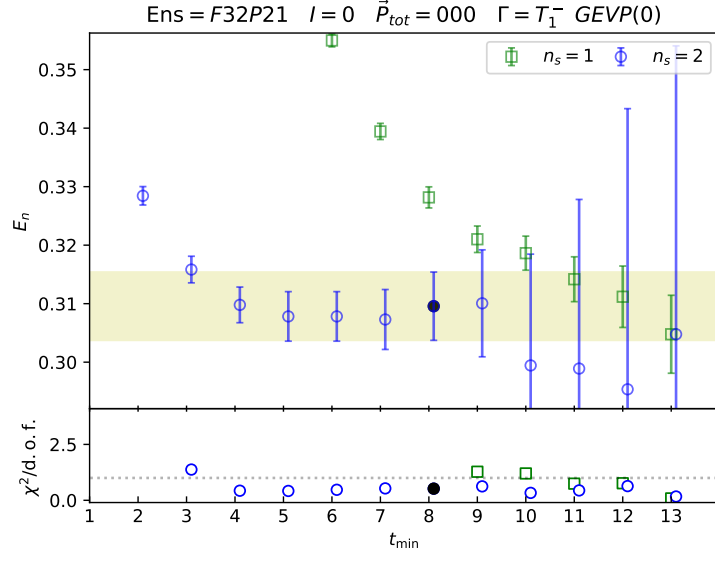FIG. S4. Effective masses of the GEVP eigenvalues in the $I = 0\,\pi\pi\pi$ channel.

FIG. S5. Stability plot for the ground state fit in the $I = 0\,\pi\pi\pi$ channel of ensemble F32P21. The blue circles are the result of the two-state fit S6, while the green squares represent the results from a one-state fit given by $\lambda_n(t, t_0) = \mathrm{e}^{-E_n(t-t_0)}$. The chosen value of $t_{\min}$ in the two-state fit is represented as a filled point.
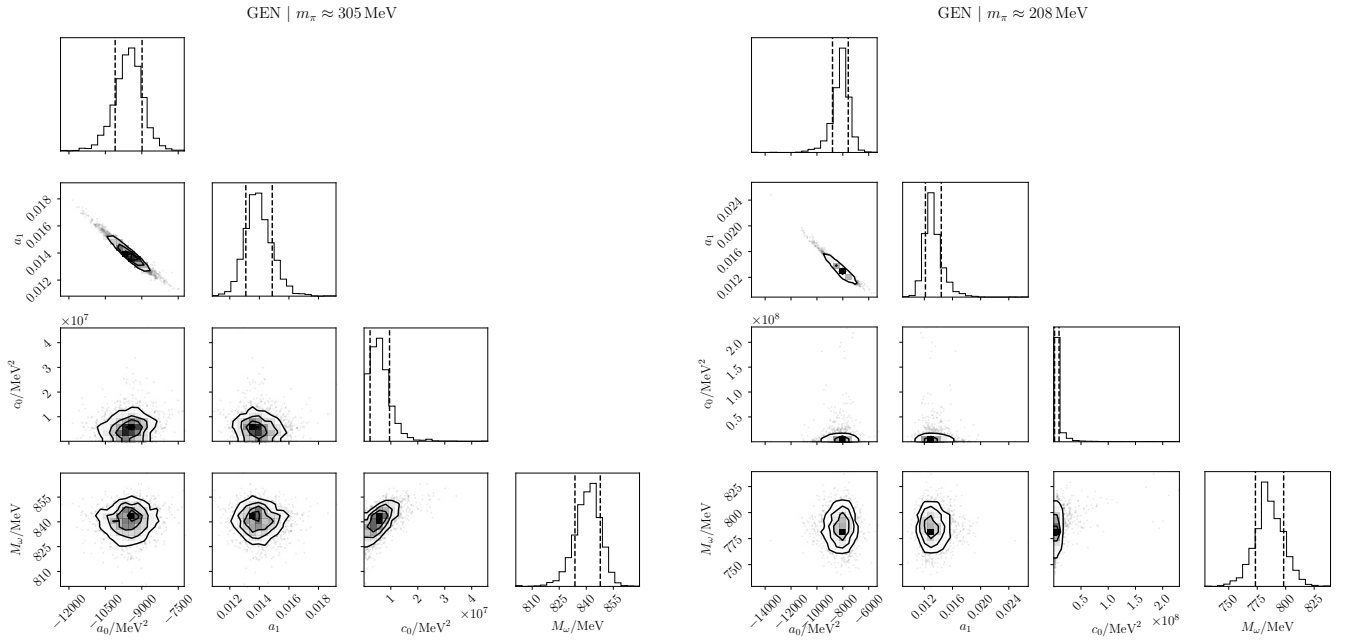

FIG. S6. Corner plots for GEN parametrizations with respect to fits at heavy (left panel) and light (right panel) pion masses.
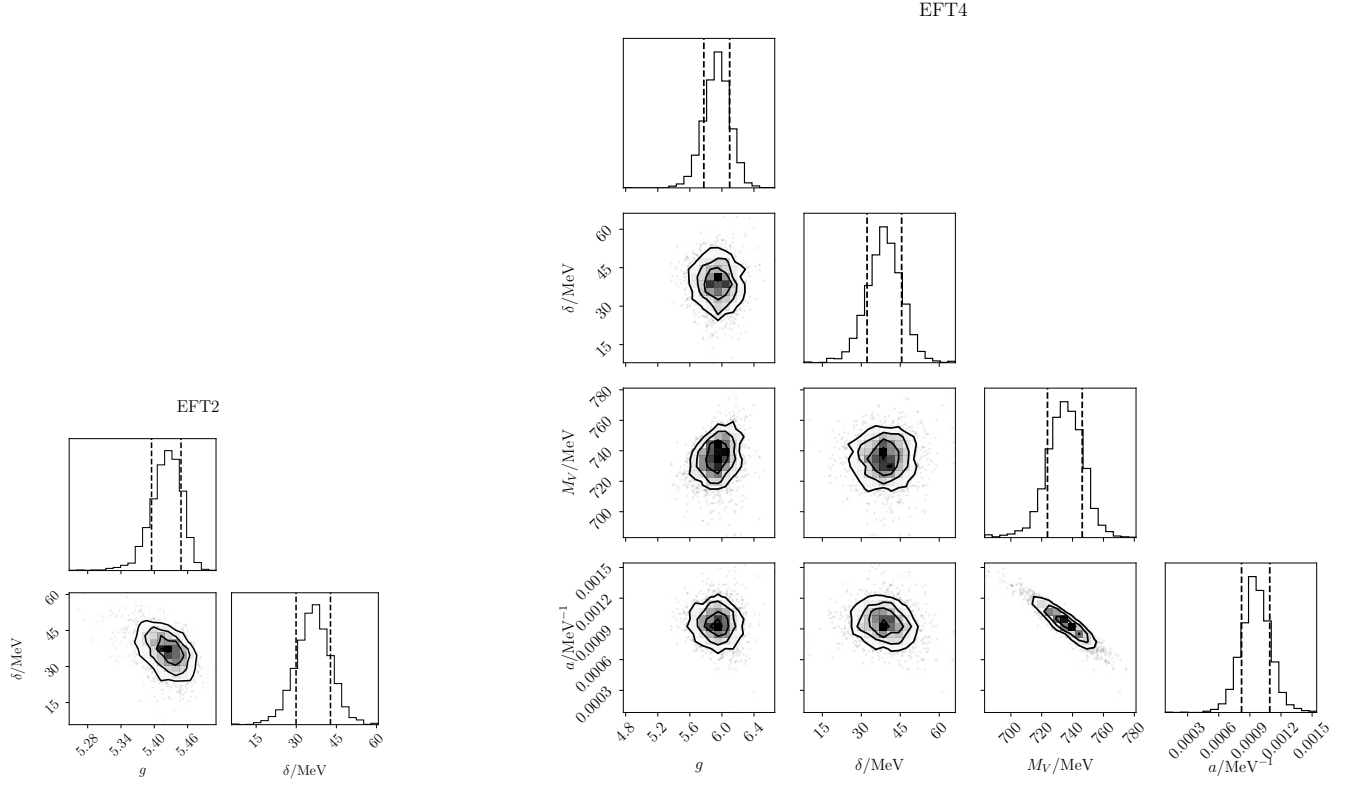
FIG. S7. Corner plots for the EFT2 (left panel) and EFT4 (right panel) parametrizations with respect to simultaneous fits to light and heavy pion mass ensembles.
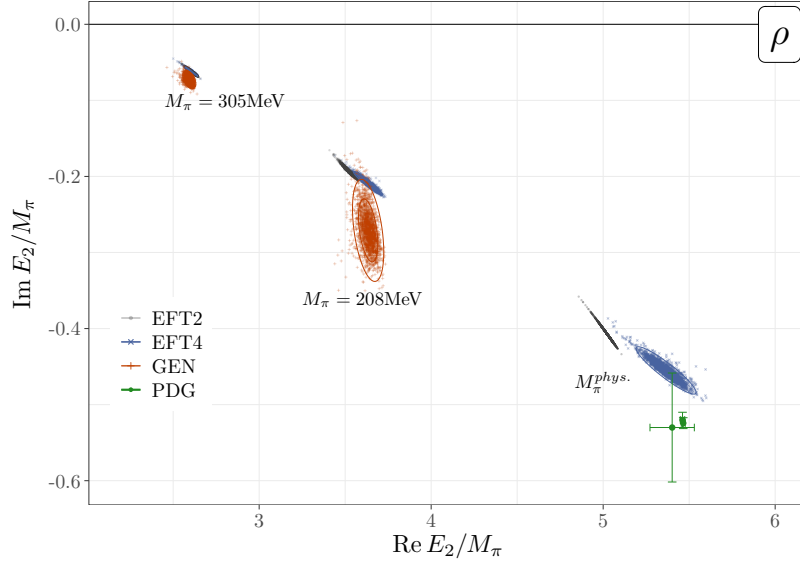

FIG. S8. Pole positions of the ρ-meson at varying pion mass from the IVU approach using generic and effective field theory form of the two- and three-body force, as described in Fig. 3 in the main text. PDG results are quoted by the green error bars for comparison [60–62, 87].